Applied Physics Letters

Optical properties of InGaN-based red multiple quantum wells

Cite as: Appl. Phys. Lett. **120**, 261102 (2022); https://doi.org/10.1063/5.0096155
Submitted: 15 April 2022 • Accepted: 17 June 2022 • Published Online: 28 June 2022

Xin Hou, Shao-Sheng Fan, Huan Xu, et al.

ARTICLES YOU MAY BE INTERESTED IN

Red InGaN micro-light-emitting diodes (>620 nm) with a peak external quantum efficiency of 4.5% using an epitaxial tunnel junction contact
Applied Physics Letters **120**, 121102 (2022); https://doi.org/10.1063/5.0086912

Influence of intrinsic or extrinsic doping on charge state of carbon and its interaction with hydrogen in GaN
Applied Physics Letters **120**, 242101 (2022); https://doi.org/10.1063/5.0093514

580-nm-thick vertical-structure light-emitting diode for visible light communication
Applied Physics Letters **120**, 181109 (2022); https://doi.org/10.1063/5.0088846

1 qubit

Shorten Setup Time
Auto-Calibration
More Qubits

Fully-integrated
Quantum Control Stacks
Ultrastable DC to 18.5 GHz
Synchronized <<1 ns
Ultralow noise

100s qubits

visit our website >

AIP Publishing

© 2022 Author(s).

Applied Physics Letters ARTICLE scitation.org/journal/apl

Optical properties of InGaN-based red multiple quantum wells

Cite as: Appl. Phys. Lett. **120**, 261102 (2022); doi: 10.1063/5.0096155
Submitted: 15 April 2022 · Accepted: 17 June 2022 ·
Published Online: 28 June 2022

Xin Hou,[1] Shao-Sheng Fan,[1] Huan Xu,[1] Daisuke Iida,[2] Yue-Jun Liu,[3] Yang Mei,[1] Guo-En Weng,[3] Shao-Qiang Chen,[3] Bao-Ping Zhang,[1,a)] and Kazuhiro Ohkawa[2]

AFFILIATIONS

[1]Laboratory of Micro/Nano-Optoelectronics, Department of Microelectronics and Integrated Circuits, Xiamen University, Xiamen 361005, China
[2]Computer, Electrical and Mathematical Sciences and Engineering (CEMSE) Division, King Abdullah University of Science and Technology (KAUST), Thuwal 23955-6900, Saudi Arabia
[3]Department of Electronic Engineering, East China Normal University, Shanghai 200241, China

[a)]Author to whom correspondence should be addressed: bzhang@xmu.edu.cn

ABSTRACT

In this work, we present the characterization of red InGaN/GaN multiple-quantum-well (MQW) light-emitting diode structures. The optical properties of two MQW structures with different n-GaN underlayer thicknesses (4 and 8 μm) are studied and compared. The results of photoluminescence studies show that a thicker n-GaN layer is beneficial for obtaining higher In content for red MQWs. However, the sample with a thicker n-GaN layer has a poorer internal quantum efficiency, a larger full width at half maximum, and a shorter nonradiative recombination time, implying that there are stronger In-content fluctuations and more defects. Furthermore, red MQWs with higher In content are shown to exhibit more deep localized states. Our findings imply that in order to achieve high-efficiency InGaN MQWs for red emission, enhancing the uniformity of In-content distribution in the active region and decreasing nonradiative recombination centers are critical challenges.

Published under an exclusive license by AIP Publishing. https://doi.org/10.1063/5.0096155

III-Nitride materials have gained a lot of research interest in recent times because of their potential in optoelectronic applications. The bandgaps of III-nitride materials cover the wavelength range from ultraviolet to near infrared by modifying the alloy composition of indium gallium nitride (InGaN) materials,[1] making them the ideal candidates for light-emitting diodes (LEDs).[2–6] Up to now, high-efficiency InGaN-based blue/green LEDs have been widely used in solid-state lighting and displays.[7–9] As a result of the rapid development of InGaN materials, researchers have started to investigate the fundamental red, green, and blue (RGB) colors using InGaN materials. In comparison to arsenide or phosphide, the InGaN material offers superior thermal stability and mechanical and chemical capabilities, and is environmentally friendly.[10] Although AlGaInP red LEDs have high efficiency and are well-established, their thermal stability is poor, and their quantum efficiency drops fast as the temperature rises. Some research groups have succeeded in producing red LEDs with a high indium content in InGaN, although they show a lower quantum efficiency than their blue and green emitting counterparts.[11,12] Therefore, several challenges must be resolved. These include large lattice mismatch,[13] the strong quantum-confined Stark effect (QCSE),[14] phase separation,[15] and the degradation of the crystal quality.[16] Controlled in-plane residual compressive stress has been shown in several studies to be an excellent strategy for improving the crystal quality of InGaN quantum wells (QWs).[17,18] Iida *et al.* demonstrated the 620 and 633-nm red LEDs[1,4] in 2016 and 2020, respectively, by lowering residual in-plane stress in the active region with a hybrid multiple-quantum-wells (MQWs) structure. Their research also showed that as the thickness of the n-GaN buffer layer increases, the in-plane residual compressive stress reduces.[1] In this approach, one could increase the In content of InGaN QWs while simultaneously improving crystal quality. Hwang *et al.*[3] reported in 2014 a 629-nm peak-wavelength InGaN-based red LED by inserting an AlGaN interlayer with a 90% Al concentration on each quantum well. This approach can achieve stress compensation and suppress the generation of mismatch dislocations. Dussaigne *et al.*[5] developed an InGaN-based red LED emitting up to 625 nm in 2021 by developing a partially relaxed $In_xGa_{1-x}N$ seed layer linked to a sapphire substrate and a buried oxide. The carrier recombination probability in the active zone of a complete

Published under an exclusive license by AIP Publishing

InGaN LED could effectively be increased by introducing an electron blocking layer. Chan *et al.*[6] produced 633-nm InGaN-based red LEDs with a high active region growth temperature of 870 °C on a relaxed InGaN/GaN superlattice buffer in 2021. Reports on studies on the development of high-In-content InGaN QW have been extensively published. However, there are just a few reports on the optical properties and carrier dynamics of InGaN with high In content, and the recombination process and carrier dynamics are still unknown.

In this work, we study the optical properties of two red MQWs epitaxial structures with different n-GaN thicknesses (4 and 8 μm) based on the work of Iida *et al.* on the in-plane residual stress. Using photoluminescence (PL) and time-resolved photoluminescence (TRPL) analyses, it is confirmed that the thicker n-GaN buffer layer is beneficial to enhance the In content in red MQWs. The thicker n-GaN buffer layer is also favorable for achieving the longer emission wavelength and deeper localized states. However, inhomogeneity due to high In content increases, and nonradiative recombination becomes a critical issue. To obtain a high-efficiency InGaN quantum well for red emission, it is necessary to increase the uniformity of In content and decrease defects. The findings from this work will help in the improvement of the crystal quality of the InGaN active layer and the development of high-efficiency long-wavelength optoelectronic devices based on nitride semiconductors.

Figure 1 shows the cross-sectional schematic of two red MQWs wafers with different n-GaN thicknesses. One 2 nm single blue QW and two 2.5 nm red QWs made up the InGaN MQWs. Meanwhile, the composition of the single blue pre-QW was set to $In_{0.2}Ga_{0.8}N$ (2 nm) with GaN(2 nm)/$Al_{0.13}Ga_{0.87}N$(18 nm)/GaN(3 nm) barrier layers. It is well known that inserting a low-indium-content pre-layer before growing high-indium-content InGaN on GaN will help to relax the strain of red QW, which helps increase indium incorporation.[19,20] The only difference between the two samples is the thickness of the n-GaN buffer layer: 4 μm (sample 1) and 8 μm (sample 2). In a prior study, Iida *et al.* have confirmed that the in-plane residual stresses of n-GaN layers with thicknesses of 4 and 8 μm are 0.54 and 0.38 GPa, respectively. The thicker n-GaN buffer layer is also conducive to reducing in-plane stress.[1] In addition, it can help the increase in In content of red MQWs. Following the work of Ohkawa *et al.*, we use temperature-dependent PL spectra and TRPL at room temperature (RT) to analyze the optical characteristics and carrier dynamics of two structures.

First, two samples were measured for temperature-dependent PL. The excitation source is a 405 nm pulsed laser with a 5 ns pulse duration and a 20 Hz repetition frequency. The spot diameter of the laser is 160 μm. For temperature-dependent PL measurements, the samples were mounted in a closed-circuit helium cryostat. The experimental temperature could be controlled from 4 to 300 K. A Princeton Instruments Model ACTONSpectrapro-3000i monochromator supplied the dispersion of the PL signal from the samples. Furthermore, TRPL measurements were performed on the two samples at room temperature. A Ti:sapphire femtosecond (fs) pulse laser was used as the excitation source which operated at 800 nm (35 fs, 1 kHz, Model Verdi G8, Coherent, America). The spot diameter of the laser is 50 μm. All the TRPL measurements were carried out at RT by a home-built confocal μ-PL system. The impulsive 400 nm pulses were generated by frequency doubling the 800 nm fs pulses using a β-barium-borate (BBO) crystal. TRPL spectra were detected by a streak-camera system (C10910, Hamamatsu, Japan) with a temporal resolution of about 10 ps. TRPL measurements were carried out similarly as described in Ref. 21.

Temperature-dependent PL measurements for both the samples showed two emission peaks (P_B and P_R). As reported earlier,[22] the P_B and P_R peaks originate from the blue pre-QW and the red MQWs, respectively. Figure 2(a) shows the PL spectra of the two samples at low temperature (4 K). The nonradiative recombination process will be inhibited at low temperatures, making these features more apparent. Sample 2 shows longer emission wavelength than sample 1, confirming red QWs have higher In content. However, the PL intensity of sample 2 is found to be weaker. In general, the PL intensity is directly proportional to the radiative recombination rate. The possibility of defect generation is lower in sample 1 due to the lower In content and lower lattice mismatch in red QWs.[23] The normalized PL of red emissions P_R in Fig. 2(b) clearly shows that sample 2's wavelength is 647.18 nm (1.916 eV), which is longer than sample 1's wavelength of 608.59 nm (2.037 eV).

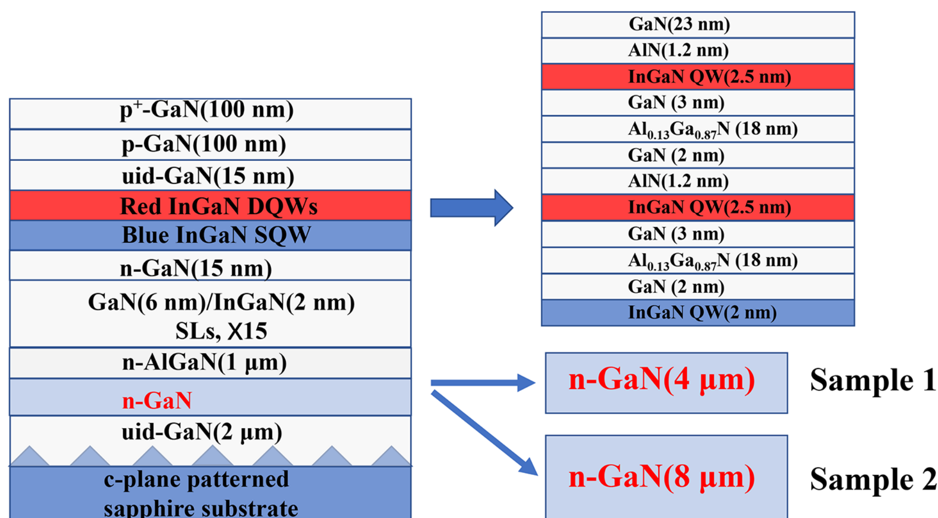

FIG. 1. Cross-sectional schematic of red InGaN-based LED structures: sample 1 with a 4-μm n-GaN layer and sample 2 with an 8-μm n-GaN layer.

Published under an exclusive license by AIP Publishing

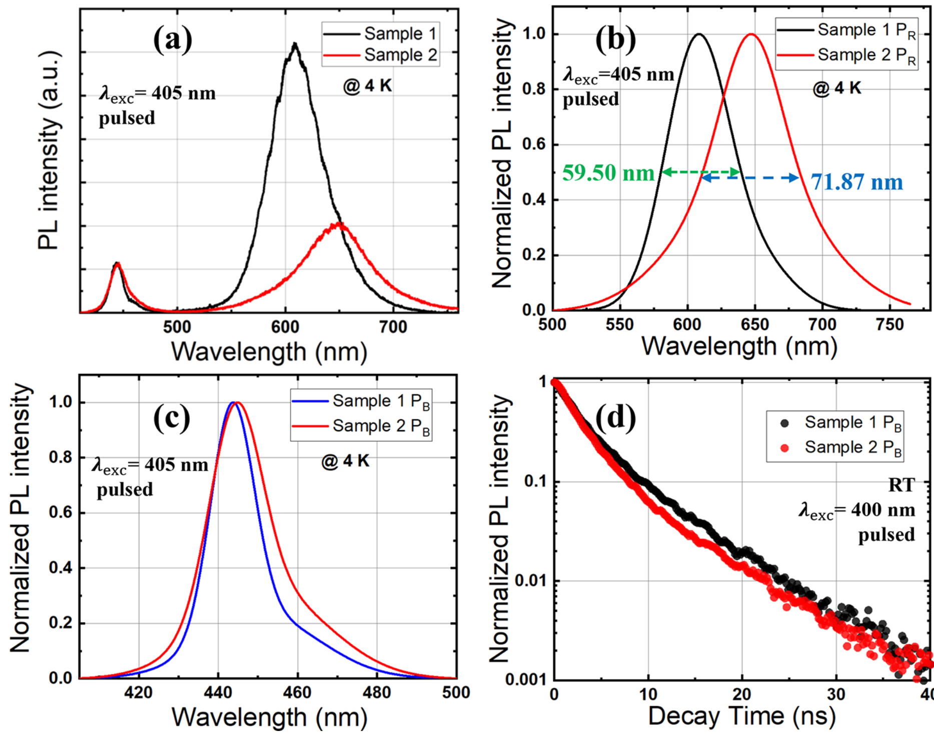

FIG. 2. (a) PL spectra of two samples, normalized PL spectra of (b) P_R and (c) P_B with excitation energy 0.3 μJ (2.98 $\times 10^2$ kW/cm^2) at low temperature (4 K); (d) the decay curves of P_B with 20 μW pumping at RT.

The notable redshift in the peak wavelength of 38.59 nm (121 meV) indicates that red double quantum wells (DQWs) in sample 2 has a higher In content. This result suggests that a thicker n-GaN buffer layer is favorable for increasing In content, which is in line with the conclusion of a prior report.[1] In addition, it is found that the full width at half maximum (FWHM) of sample 1 and sample 2 is 59.50 and 71.87 nm, respectively. Through the different PL peak wavelength in Fig. 2(b), we calculated the difference of bandgap (ΔE_g) and In content (Δx) in red QWs of two samples. The calculation formula is as follows:[22]

$$E_g(T) = E_g(T=0) - \frac{\alpha T^2}{T+\beta}, \tag{1}$$

$$E_g(\mathrm{In}_{(1-x)}\mathrm{Ga}_{(x)}\mathrm{N}) = (1-x)E_g(\mathrm{InN}) + xE_g(\mathrm{GaN}) - x(1-x)C, \tag{2}$$

where T is 4 K, $\alpha = 1.799$ meV/K, $\beta = 51462$ K, and C is a bowing parameter, which reflects a reduction of the alloy energy gap. The energy gaps of two samples are $E_{g1} = 2.037$ eV (sample 1) and $E_{g2} = 1.916$ eV (sample 2). The bandgap difference of two samples is $\Delta E_g = 121$ meV. At the same time, the In content of two samples is $x_1 = 0.4008$ (sample 1) and $x_2 = 0.4431$ (sample 2). The In-content difference of two samples is about $\Delta x = 0.0423$, which indicates a slight In-content difference.

The higher In content, however, leads to high In fluctuation in red DQWs, which will be discussed later. As for the blue emission P_B, sample 2 shows a longer peak wavelength and wider FWHM, which indicates that it is higher In content and also larger In fluctuation (in sample 2), as shown in Fig. 2(c). The P_B was further examined by TRPL at room temperature. Figure 2(d) shows the P_B decay curves of the two samples. The decay curve from sample 2 is faster, indicating that sample 2 has more nonradiative recombination.

To further study the stress adjustment caused by the thick n-GaN buffer layer in the red active region, temperature-dependent PL spectra of samples 1 and 2 were investigated in the temperature range 15–300 K. As shown in Fig. 3, the internal quantum efficiency (IQE) of the two samples was obtained from the variation of the

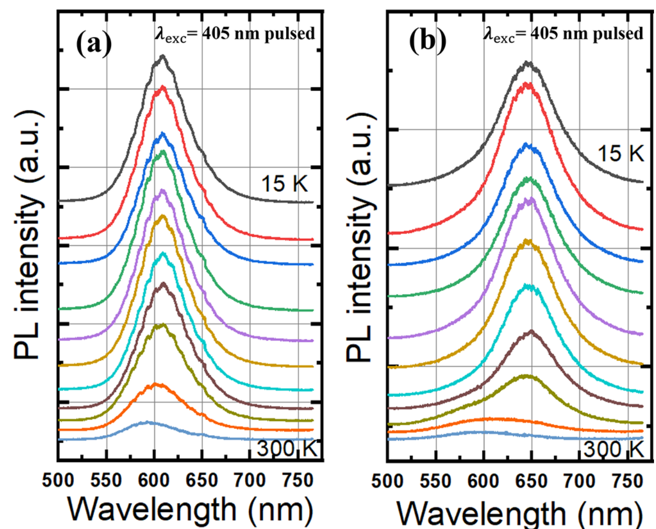

FIG. 3. The dependent-temperature PL spectra of (a) sample 1 and (b) sample 2 with 15–300 K.

Published under an exclusive license by AIP Publishing

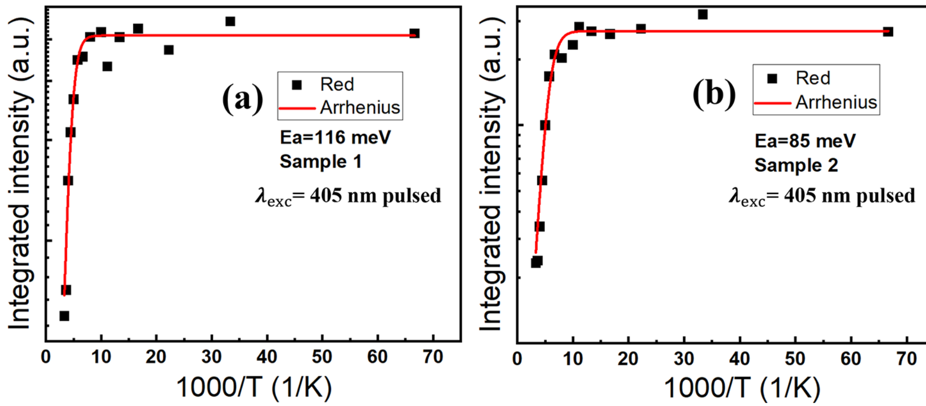

FIG. 4. Arrhenius plots of red emission P_R intensity vs temperature of (a) sample 1 and (b) sample 2.

temperature-dependent PL intensities. The IQE is typically accepted and utilized as the ratio of integrated PL intensity between ambient temperature (300 K) and 15 K.[23–26] The IQE of samples 1 and 2 was found to be 24.03% and 13.53%, respectively. Sample 2 shows a lower value of IQE.

To further investigate the influence of nonradiative recombination in the red active region, we use the one-channel Arrhenius model to fit the temperature-dependent PL intensities of both the samples.[23] This technique can be used to quantitatively study the activation energy of the corresponding nonradiative centers using the following equation:

$$I(T) = \frac{I_0}{\left[1 + A \times \exp\left(-\frac{E_a}{k_B \times T}\right)\right]}, \tag{3}$$

where I_0 is the integrated PL intensity at low temperature, A is the constant related to the density of nonradiative recombination centers, E_a is the activation energy of the corresponding nonradiative centers induced by defects, and k_B is the Boltzmann constant. The fitted curves are shown in Fig. 4. From the above Eq. (1), the values of E_a for samples 1 and 2 are found to be 116 and 85 meV, respectively. These data demonstrate that the nonradiative recombination centers are easily activated in red MQWs of sample 2.

In addition, the TRPL curves at the peak energy are fitted by two exponential functions. The equation is as follows:[27,28]

$$I(t) = B_1 \times \exp\left(\frac{-t}{\tau_1}\right) + B_2 \times \exp\left(\frac{-t}{\tau_2}\right), \tag{4}$$

where $I(t)$ is the TRPL intensity at time t. The parameters τ_1 and τ_2 are the fast decay time and slow decay time, respectively. As shown in Fig. 5, the rate of decay in sample 2 is faster, and the decay time is also shorter. By fitting, the τ_1 and τ_2 of sample 1 were found to be 10.02 and 24.78 ns, respectively. The τ_1 and τ_2 of sample 2 were found to be 4.708 and 14.67 ns, respectively. Sample 2 shows shorter decay times and lower IQE, which also indicates that the nonradiative recombination is more pronounced.

Carrier transfer from weak to strongly localized states is generally attributed to the early rapid decay phase, whereas carrier recombination in strongly localized states is assigned to the slow decay process.[17] In-rich clusters and quasi-quantum dot formations, in which the In content is higher than the average value in InGaN QW, result in localized states. Combined IQE and the slow decay times of TRPL, the radiative recombination time (τ_{2r}) and the nonradiative recombination time (τ_{2nr}) are calculated by the following equations:[27]

$$\frac{1}{\tau_2} = \frac{1}{\tau_{2r}} + \frac{1}{\tau_{2nr}}, \tag{5}$$

$$\tau_{2r} = \tau_2 \times \frac{1}{\eta}, \tag{6}$$

$$\tau_{2nr} = \tau_2 \times \frac{1}{1-\eta}. \tag{7}$$

The nonradiative recombination times of sample 1 and 2 are 32.62 and 16.97 ns, respectively. The detailed data of the two samples are listed in Table I. It is noted that the nonradiative recombination time

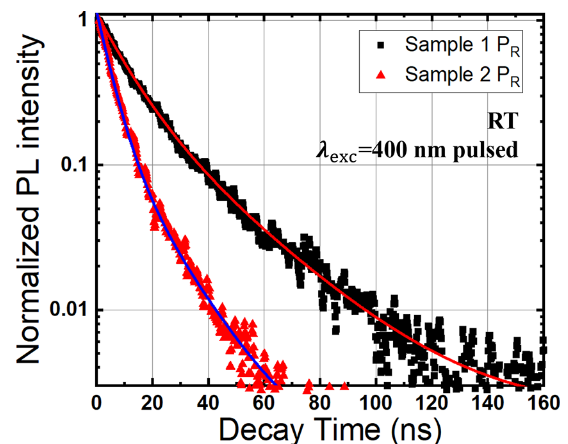

FIG. 5. TRPL curves and fitting results of red emission P_R for two samples with 20 μW pumping (3.39×10^6 kW/cm^2).

TABLE I. η, τ_2, τ_{2r}, and τ_{2nr} of two samples.

Sample	η	τ_2 (ns)	τ_{2r} (ns)	τ_{2nr} (ns)
Sample 1	24.03%	24.78	103.1	32.62
Sample 2	13.53%	14.67	108.4	16.97

Published under an exclusive license by AIP Publishing

of sample 2 is shorter, indicating that the nonradiative recombination affects heavily the carrier recombination process. This result is in agreement with the smaller activation energy of the corresponding nonradiative centers.

The PL spectra of the two samples at different decay times (3, 5, 8, 15, 30, 40, 70, and 100 ns) show that the peak wavelength shift of sample 2 is larger than that of sample 1. As shown in Fig. 6, the wavelength shift of samples 1 and 2 is 34.49 and 61.79 nm, respectively. This phenomenon illustrates that the red DQWs of sample 2 show a stronger localized effect and deeper localized states. Using Fig. 6, we calculate the PL redshift of two samples at decay times 3 and 100 ns. $\Delta E_1 = 125$ meV (sample 1), $\Delta E_2 = 221$ meV (sample 2). Comparing ΔE_1 and ΔE_2, it indicates that the In fluctuation of sample 2 is larger, and the maximum In content of In clusters is larger too. Figure 6 also shows that the higher In content causes a larger inhomogeneity and a wider FWHM of the red emission peak of sample 2, being in agreement with the results shown in Fig. 2(b). Therefore, In uniformity will be a challenge in reducing the FWHM of PL in InGaN red MQWs.

On the contrary, the built-in electric fields of red QWs under two extreme conditions are calculated, including complete relaxation and complete strain. The electric field can be written as the difference of the polarization (PZ) in the barriers and wells, given by[29]

$$F_W = (P_{sp}^b + P_{pz}^b - P_{sp}^w - P_{pz}^w)/\varepsilon_0\varepsilon_w, \quad (8)$$

where P_{sp}^b (P_{sp}^w) and P_{pz}^b(P_{pz}^w) are the spontaneous polarization (SP) and piezoelectric polarization (PZ) of the barrier (well), respectively. F_W is the field strength, and ε_0 and ε_w are, respectively, the vacuum permittivity (8.854×10^{-12}) and the relative permittivity (12.78) of the InGaN well. The built-in electric fields of complete relaxation and complete strain are 0.07 and 0.37 MV/cm, respectively. It means that the built-in electric field, causing QCSE, is about 0.07–0.37 MV/cm.

At the minimum excitation energy of 0.06 μJ (59.7 kW/cm^2), the red peak wavelengths are 617.93 (sample 1) and 651.33 nm (sample 2). The carrier density is small, and there is no screening of the QCSE. When there is no In fluctuation, the built-in electric fields of two samples were calculated by peak wavelength of the red QWs, given by[30]

$$E_{1e-1h} = E_g - F_w L_w + \left[9\pi\hbar F_w/(8\sqrt{2})\right]^{2/3}(1/m_e^* + 1/m_h^*)^{1/3}, \quad (9)$$

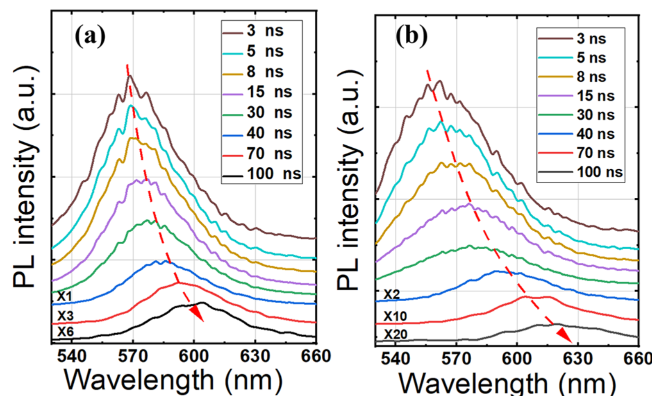

FIG. 6. The PL spectra of (a) sample 1 and (b) sample 2 at different decay times with 400 nm pulsed laser.

where E_g is the bandgap of InGaN, F_W, L_w, m_e^*, and m_h^* are the polarization field, well width (2.5 nm), and electron- and hole-effective mass of InGaN well, respectively. E_{1e-1h} is the transition energy between the first electron level and the first hole level. Numerical calculation by Eq. (9) shows that the built-in electric field of sample 1 is 1.37 MV/cm, and that of sample 2 is 1.78 MV/cm, which are much larger than strain-induced electric field given above. In other words, In fluctuation must be considered. It shows that the PL redshift is mainly caused by the In fluctuation, and QCSE plays a negligible role.

In summary, using PL and TRPL measurements and detailed analyses, we show that a thicker n-GaN layer is desirable to boost In content for achieving the red emission. However, the lower IQE and wider FWHM indicate that a higher In content results in more defects and inhomogeneity in In composition. The blue single QW also shows similar results. At the same time, nonradiative recombination has a greater impact on carrier dynamics in higher-In-content QWs. The substantial lattice mismatch between the higher In-content InGaN layer and the GaN barrier should be responsible for this problem. To produce high-efficiency red InGaN quantum wells, it is necessary to increase the uniformity of the In composition and decrease defects as well. Growing red InGaN wells atop a strain-relaxed InGaN layer with similar In content could be a promising option to reduce the strain and the built-in electric field in the well layer. Using pre-layers is also beneficial to enhance the In uniformity, reduce the localized states and PL FWHM, and expand the free movement space of electrons and holes, increasing the probability of radiation recombination.[4] The experimental results presented may provide a guideline for synthesizing high-In-content InGaN active layers.

This work was supported by the National Key Research and Development Program of China (No. 2017YFE0131500) and the National Natural Science Foundation of China (Nos. 62104204 and U21A20493). The authors would like to thank Zhong-Ming Zheng, Lei-Ying Ying, Zhi-Wei Zheng, and Hao Long of Xiamen University for support and useful discussions.

AUTHOR DECLARATIONS

Conflict of Interest

The authors have no conflicts to disclose.

Author Contributions

Xin Hou: Conceptualization (equal); Data curation (equal); Investigation (equal); Writing – original draft (equal); Writing – review and editing (equal). **Shao-Sheng Fan:** Data curation (equal). **Huan Xu:** Methodology (supporting). **Daisuke Iida:** Data curation (equal); Methodology (equal). **Yue-Jun Liu:** Investigation (supporting). **Yang Mei:** Project administration (supporting). **Guo-En Weng:** Data curation (supporting). **Shao-Qiang Chen:** Data curation (supporting). **Bao-Ping Zhang:** Funding acquisition (lead); Project administration (lead); Supervision (lead); Writing – review and editing (equal). **Kazuhiro Ohkawa:** Investigation (equal); Resources (equal); Supervision (equal); Writing – review and editing (equal).

DATA AVAILABILITY

The data that support the findings of this study are available from the corresponding author upon reasonable request.

Published under an exclusive license by AIP Publishing

REFERENCES

[1] D. Iida, Z. Zhuang, P. Kirilenko, M. Velazquez-Rizo, M. A. Najmi, and K. Ohkawa, "633-nm InGaN-based red LEDs grown on thick underlying GaN layers with reduced in-plane residual stress," Appl. Phys. Lett. **116**, 162101 (2020).

[2] M. Pophristic, F. H. Long, C. Tran, R. F. Karlicek, Z. C. Feng, and I. T. Ferguson, "Time-resolved spectroscopy of $In_xGa_{1-x}N$/GaN multiple quantum wells at room temperature," Appl. Phys. Lett. **73**, 815–817 (1998).

[3] J. I. Hwang, R. Hashimoto, S. Saito, and S. Nunoue, "Development of InGaN-based red LED grown on (0001) polar surface," Appl. Phys. Express **7**, 071003 (2014).

[4] D. Iida, K. Niwa, S. Kamiyama, and K. Ohkawa, "Demonstration of InGaN-based orange LEDs with hybrid multiple-quantum-wells structure," Appl. Phys. Express **9**, 111003 (2016).

[5] A. Dussaigne, P. L. Maitre, H. Haas, J. C. Pillet, F. Barbier, A. Grenier, N. Michit, A. Jannaud, R. Templier, D. Vaufrey, F. Rol, O. Ledoux, and D. Sotta, "Full InGaN red (625 nm) micro-LED (10 μm) demonstration on a relaxed pseudo-substrate," Appl. Phys. Express **14**, 092011 (2021).

[6] P. Chan, V. Rienzi, N. Lim, H. M. Chang, M. Gordon, S. P. DenBaars, and S. Nakamura, "Demonstration of relaxed InGaN-based red LEDs grown with high active region temperature," Appl. Phys. Express **14**, 101002 (2021).

[7] D. S. Arteev, A. V. Sakharov, A. E. Nikolaev, W. V. Lundin, and A. F. Tsatsulnikov, "Temperature-dependent luminescent properties of dual-wavelength InGaN LEDs," J. Lumin. **234**, 117957 (2021).

[8] R. B. Xu, H. Xu, Y. Mei, X. L. Shi, L. Y. Ying, Z. W. Zheng, H. Long, Z. R. Qiu, B. P. Zhang, J. P. Liu, and H. C. Kuo, "Emission dynamics of GaN-based blue resonant-cavity light-emitting diodes," J. Lumin. **216**, 116717 (2019).

[9] T. Shioda, H. Yoshida, K. Tachibana, N. Sugiyama, and S. Nunoue, "Enhanced light output power of green LEDs employing AlGaN interlayer in InGaN/GaN MQW structure on sapphire (0001) substrate," Phys. Status Solidi A **209**(3), 473–476 (2012).

[10] S. N. Zhang, J. L. Zhang, J. D. Gao, X. L. Wang, C. D. Zheng, M. Zhang, X. M. Wu, L. Q. Xu, J. Ding, Z. J. Quan, and F. Y. Jiang, "Efficient emission of InGaN-based light-emitting diodes: Toward orange and red," Photonics Res. **8**, 1671–1675 (2020).

[11] Z. Zhuang, D. Iida, and K. Ohkawa, "Ultrasmall and ultradense InGaN-based RGB monochromatic micro-light-emitting diode arrays by pixilation of conductive p-GaN," Photonics Res. **9**, 2429–2434 (2021).

[12] B. Damilano and B. Gil, "Yellow-red emission from (Ga, In) N heterostructures," J. Phys. D **48**, 403001 (2015).

[13] Y. Yamashita, H. Tamura, N. Horio, H. Sato, K. Taniguchi, T. Chinone, S. Omori, and C. Funaoka, "Control of emission wavelength of GaInN single quantum well, light emitting diodes grown by metalorganic chemical vapor deposition in a split-flow reactor," Jpn. J. Appl. Phys., Part 1 **42**, 4197–4197 (2003).

[14] Z. Zhuang, D. Iida, M. Velazquez-Rizo, and K. Ohkawa, "606-nm InGaN amber micro-light-emitting diodes with an on-wafer external quantum efficiency of 0.56%," IEEE Electron Device Lett. **42**, 1029–1032 (2021).

[15] T. Mukai, M. Yamada, and S. Nakamura, "Characteristics of InGaN-based UV/blue/green/amber/red light-emitting diodes," Jpn. J. Appl. Phys., Part 1 **38**, 3976–3981 (1999).

[16] Y. J. Zhao, S. Ho Oh, F. Wu, Y. Kawaguchi, S. Tanaka, K. Fujito, J. S. Speck, S. P. DenBaars, and S. Nakamura, "Green semipolar ($20\bar{2}\bar{1}$) InGaN light-emitting diodes with small wavelength shift and narrow spectral linewidth," Appl. Phys. Express **6**, 062102 (2013).

[17] M. C. Johnson, E. D. Bourret-Courchesne, J. Wu, Z. Liliental-Weber, D. N. Zakharov, R. J. Jorgenson, T. B. Ng, D. E. McCready, and J. R. Williams, "Effect of gallium nitride template layer strain on the growth of $In_xGa_{1-x}N$/GaN multiple quantum well light emitting diodes," J. Appl. Phys. **96**, 1381–1386 (2004).

[18] C. Roeder, F. Lipski, F. Habel, G. Leibiger, M. Abendroth, C. Himcinschi, and J. Kortus, "Raman spectroscopic characterization of epitaxially grown GaN on sapphire," J. Phys. D **46**, 285302 (2013).

[19] D. Iida, S. Lu, S. Hirahara, K. Niwa, S. Kamiyama, and K. Ohkawa, "Enhanced light output power of InGaN-based amber LEDs by strain-compensating AlN/AlGaN barriers," J. Cryst. Growth **448**, 105–108 (2016).

[20] J. L. Zhang, C. B. Xiong, J. L. Liu, Z. J. Quan, L. Wang, and F. Y. Jiang, "High brightness InGaN-based yellow light-emitting diodes with strain modulation layers grown on Si substrate," Appl. Phys. A **114**, 1049–1053 (2014).

[21] G. E. Weng, J. Y. Yan, S. J. Chen, C. H. Zhao, H. B. Zhang, J. Tian, Y. J. Liu, X. B. Hu, J. H. Tao, S. Q. Chen, Z. Q. Zhu, H. Akiyama, and J. H. Chu, "Superior single-mode lasing in self-assembly $CsPbX_3$ microcavity over an ultrawide pumping wavelength range," Photonics Res. **9**, 54–65 (2021).

[22] I. Vurgaftman and J. R. Meyer, "Band parameters for nitrogen-containing semiconductors," J. Appl. Phys. **94**(6), 3675–3696 (2003).

[23] X. Hou, S. S. Fan, D. Iida, Y. Mei, B. P. Zhang, and K. Ohkawa, "Photoluminescence of InGaN-based red multiple quantum wells," Opt. Express **29**, 30237–30243 (2021).

[24] Z. Zhuang, D. Iida, and K. Ohkawa, "InGaN-based red light-emitting diodes: From traditional to micro-LEDs," Jpn. J. Appl. Phys., Part 1 **61**, SA0809 (2022).

[25] Y. L. Lai, C. P. Liu, Y. H. Lin, T. H. Hsueh, R. M. Lin, D. Y. Lyu, Z. X. Peng, and T. Y. Lin, "Origins of efficient green light emission in phase-separated InGaN quantum wells," Nanotechnology **17**, 3734–3739 (2006).

[26] R. Li, M. S. Xu, P. Wang, C. X. Wang, S. D. Qu, K. J. Shi, Y. H. Wei, X. G. Xu, and Z. W. Ji, "Combined effects of carrier scattering and Coulomb screening on photoluminescence in InGaN/GaN quantum well structure with high In content," Chin. Phys. B **30**, 047801 (2021).

[27] L. Wang, Y. C. Xing, Z. B. Hao, and Y. Luo, "Study on carrier lifetimes in InGaN multi-quantum well with different barriers by time-resolved photoluminescence," Phys. Status Solidi B **252**, 956–960 (2015).

[28] G. E. Weng, W. R. Zhao, S. Q. Chen, H. Akiyama, Z. C. Li, J. P. Liu, and B. P. Zhang, "Strong localization effect and carrier relaxation dynamics in self-assembled InGaN quantum dots emitting in the green," Nanoscale Res. Lett. **10**, 31 (2015).

[29] Q. Guo, R. Kirste, S. Mita, J. Tweedie, P. Reddy, S. Washiyama, M. H. Breckenridge, R. Collazo, and Z. Sitar, "The polarization field in Al-rich AlGaN multiple quantum wells," Jpn. J. Appl. Phys., Part 1 **58**, SCCC10 (2019).

[30] J. Li, S. Li, and J. Kang, "Quantized level transitions and modification in InGaN/GaN multiple quantum wells," Appl. Phys. Lett. **92**(10), 101929 (2008).

Published under an exclusive license by AIP Publishing